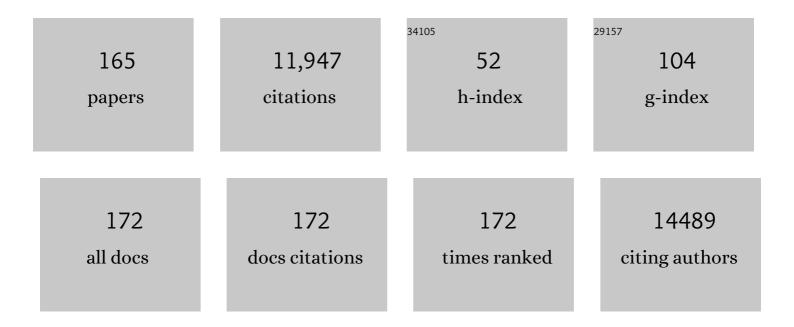
List of Publications by Year in descending order

Source: https://exaly.com/author-pdf/9122023/publications.pdf Version: 2024-02-01



#	Article	IF	CITATIONS
1	Perovskite light-emitting diodes based on spontaneously formed submicrometre-scale structures. Nature, 2018, 562, 249-253.	27.8	1,555
2	Nickel–vanadium monolayer double hydroxide for efficient electrochemical water oxidation. Nature Communications, 2016, 7, 11981.	12.8	808
3	Thermochromic halide perovskite solar cells. Nature Materials, 2018, 17, 261-267.	27.5	630
4	Direct Observation of Structural Evolution of Metal Chalcogenide in Electrocatalytic Water Oxidation. ACS Nano, 2018, 12, 12369-12379.	14.6	366
5	Vacancyâ€Rich Monolayer BiO _{2â^`<i>x</i>} as a Highly Efficient UV, Visible, and Nearâ€Infrared Responsive Photocatalyst. Angewandte Chemie - International Edition, 2018, 57, 491-495.	13.8	365
6	Highâ€Energy/Power and Lowâ€Temperature Cathode for Sodiumâ€Ion Batteries: In Situ XRD Study and Superior Fullâ€Cell Performance. Advanced Materials, 2017, 29, 1701968.	21.0	350
7	Dendritic core-shell nickel-iron-copper metal/metal oxide electrode for efficient electrocatalytic water oxidation. Nature Communications, 2018, 9, 381.	12.8	322
8	Oriented Quasiâ€2D Perovskites for High Performance Optoelectronic Devices. Advanced Materials, 2018, 30, e1804771.	21.0	268
9	Single-Atom Fe Catalyst Outperforms Its Homogeneous Counterpart for Activating Peroxymonosulfate to Achieve Effective Degradation of Organic Contaminants. Environmental Science & Technology, 2021, 55, 7034-7043.	10.0	244
10	Liquid medium annealing for fabricating durable perovskite solar cells with improved reproducibility. Science, 2021, 373, 561-567.	12.6	227
11	Photocatalytic CO ₂ Conversion of M _{0.33} WO ₃ Directly from the Air with High Selectivity: Insight into Full Spectrum-Induced Reaction Mechanism. Journal of the American Chemical Society, 2019, 141, 5267-5274.	13.7	224
12	Hollow Iron–Vanadium Composite Spheres: A Highly Efficient Ironâ€Based Water Oxidation Electrocatalyst without the Need for Nickel or Cobalt. Angewandte Chemie - International Edition, 2017, 56, 3289-3293.	13.8	216
13	Rational design of infrared nonlinear optical chalcogenides by chemical substitution. Coordination Chemistry Reviews, 2020, 406, 213150.	18.8	194
14	Organic Polymer Dots as Photocatalysts for Visible Lightâ€Driven Hydrogen Generation. Angewandte Chemie - International Edition, 2016, 55, 12306-12310.	13.8	191
15	Interfacial Engineering of Bi ₁₉ Br ₃ S ₂₇ Nanowires Promotes Metallic Photocatalytic CO ₂ Reduction Activity under Near-Infrared Light Irradiation. Journal of the American Chemical Society, 2021, 143, 6551-6559.	13.7	159
16	Series of Highly Stable Isoreticular Lanthanide Metal–Organic Frameworks with Expanding Pore Size and Tunable Luminescent Properties. Chemistry of Materials, 2015, 27, 5332-5339.	6.7	146
17	The effect of the polyaniline morphology on the performance of polyaniline supercapacitors. Journal of Solid State Electrochemistry, 2005, 9, 574-580.	2.5	139
18	A nickel (II) PY5 complex as an electrocatalyst for water oxidation. Journal of Catalysis, 2016, 335, 72-78.	6.2	121

#	Article	IF	CITATIONS
19	Full spectrum light driven photocatalytic in-situ epitaxy of one-unit-cell Bi2O2CO3 layers on Bi2O4 nanocrystals for highly efficient photocatalysis and mechanism unveiling. Applied Catalysis B: Environmental, 2019, 243, 667-677.	20.2	114
20	PbGa ₂ MSe ₆ (M = Si, Ge): Two Exceptional Infrared Nonlinear Optical Crystals. Chemistry of Materials, 2015, 27, 914-922.	6.7	110
21	Tuning electronic property and surface reconstruction of amorphous iron borides via W-P co-doping for highly efficient oxygen evolution. Applied Catalysis B: Environmental, 2021, 288, 120037.	20.2	108
22	Efficient and bright warm-white electroluminescence from lead-free metal halides. Nature Communications, 2021, 12, 1421.	12.8	99
23	Synthesis of Silver Nanowires with Reduced Diameters Using Benzoin-Derived Radicals to Make Transparent Conductors with High Transparency and Low Haze. Nano Letters, 2018, 18, 5329-5334.	9.1	96
24	A Zn-MOF constructed from electron-rich π-conjugated ligands with an interpenetrated graphene-like net as an efficient nitroaromatic sensor. RSC Advances, 2016, 6, 45475-45481.	3.6	94
25	Zeolite A synthesized from alkaline assisted pre-activated halloysite for efficient heavy metal removal in polluted river water and industrial wastewater. Journal of Environmental Sciences, 2017, 56, 254-262.	6.1	91
26	High conductivity Ag-based metal organic complexes as dopant-free hole-transport materials for perovskite solar cells with high fill factors. Chemical Science, 2016, 7, 2633-2638.	7.4	89
27	Structural and spectral dynamics of single-crystalline Ruddlesden-Popper phase halide perovskite blue light-emitting diodes. Science Advances, 2020, 6, eaay4045.	10.3	88
28	Infrared SHG Materials CsM ₃ Se ₆ (M = Ga/Sn, In/Sn): Phase Matchability Controlled by Dipole Moment of the Asymmetric Building Unit. Chemistry of Materials, 2017, 29, 499-503.	6.7	87
29	Plasmonic MoO3-x nanosheets with tunable oxygen vacancies as efficient visible light responsive photocatalyst. Applied Surface Science, 2019, 490, 395-402.	6.1	86
30	Selective CO2 photoreduction to CH4 mediated by dimension-matched 2D/2D Bi3NbO7/g-C3N4 S-scheme heterojunction. Chinese Journal of Catalysis, 2022, 43, 246-254.	14.0	85
31	Partial Isovalent Anion Substitution to Access Remarkable Second-Harmonic Generation Response: A Generic and Effective Strategy for Design of Infrared Nonlinear Optical Materials. Chemistry of Materials, 2020, 32, 5890-5896.	6.7	84
32	Salt-Inclusion Chalcogenide [Ba ₄ Cl ₂][ZnGa ₄ S ₁₀]: Rational Design of an IR Nonlinear Optical Material with Superior Comprehensive Performance Derived from AgGaS ₂ . Chemistry of Materials, 2020, 32, 8012-8019.	6.7	83
33	Cu(II) Complexes as p-Type Dopants in Efficient Perovskite Solar Cells. ACS Energy Letters, 2017, 2, 497-503.	17.4	77
34	Re-Investigation of Cobalt Porphyrin for Electrochemical Water Oxidation on FTO Surface: Formation of CoOx as Active Species. ACS Catalysis, 2017, 7, 1143-1149.	11.2	74
35	Bi ₂ O ₃ /BiO ₂ Nanoheterojunction for Highly Efficient Electrocatalytic CO ₂ Reduction to Formate. Nano Letters, 2022, 22, 1656-1664.	9.1	72
36	A Tailorâ€Made Molecular Ruthenium Catalyst for the Oxidation of Water and Its Deactivation through Poisoning by Carbon Monoxide. Angewandte Chemie - International Edition, 2013, 52, 4189-4193.	13.8	69

#	Article	IF	CITATIONS
37	Solidâ€State Perovskiteâ€Sensitized pâ€Type Mesoporous Nickel Oxide Solar Cells. ChemSusChem, 2014, 7, 2150-2153.	6.8	69
38	A Germanosilicate Structure with 11×11×12â€Ring Channels Solved by Electron Crystallography. Angewandte Chemie - International Edition, 2014, 53, 5868-5871.	13.8	69
39	Promoting the Water Oxidation Catalysis by Synergistic Interactions between Ni(OH) ₂ and Carbon Nanotubes. Advanced Energy Materials, 2016, 6, 1600516.	19.5	68
40	General Post-annealing Method Enables High-Efficiency Two-Dimensional Perovskite Solar Cells. ACS Applied Materials & Interfaces, 2018, 10, 33187-33197.	8.0	66
41	Bis(1,1-bis(2-pyridyl)ethane)copper(<scp>i</scp> / <scp>ii</scp>) as an efficient redox couple for liquid dye-sensitized solar cells. Journal of Materials Chemistry A, 2016, 4, 14550-14554.	10.3	63
42	Defective and " <i>c</i> -Disordered― <i>Hortensia</i> -like Layered MnO _{<i>x</i>} as an Efficient Electrocatalyst for Water Oxidation at Neutral pH. ACS Catalysis, 2017, 7, 6311-6322.	11.2	62
43	3D Open-Framework Vanadoborate as a Highly Effective Heterogeneous Pre-catalyst for the Oxidation of Alkylbenzenes. Chemistry of Materials, 2013, 25, 5031-5036.	6.7	61
44	N-doping induced tensile-strained Pt nanoparticles ensuring an excellent durability of the oxygen reduction reaction. Journal of Catalysis, 2020, 382, 247-255.	6.2	61
45	Highly efficient phenothiazine 5,5-dioxide-based hole transport materials for planar perovskite solar cells with a PCE exceeding 20%. Journal of Materials Chemistry A, 2019, 7, 9510-9516.	10.3	60
46	Unlocking bimetallic active sites via a desalination strategy for photocatalytic reduction of atmospheric carbon dioxide. Nature Communications, 2022, 13, 2146.	12.8	60
47	Integrated Design of Organic Hole Transport Materials for Efficient Solidâ€State Dyeâ€Sensitized Solar Cells. Advanced Energy Materials, 2015, 5, 1401185.	19.5	59
48	Mixed Redox-Couple-Involved Chalcopyrite Phase CuFeS ₂ Quantum Dots for Highly Efficient Cr(VI) Removal. Environmental Science & Technology, 2020, 54, 8022-8031.	10.0	57
49	Recent advances in waste-derived functional materials for wastewater remediation. , 2022, 1, 86-104.		57
50	Molecular engineering for efficient and selective iron porphyrin catalysts for electrochemical reduction of CO ₂ to CO. Chemical Communications, 2016, 52, 14478-14481.	4.1	55
51	Experimental and theoretical studies on the NLO properties of two quaternary non-centrosymmetric chalcogenides: BaAg ₂ GeS ₄ and BaAg ₂ SnS ₄ . Dalton Transactions, 2018, 47, 429-437.	3.3	55
52	Control of Barrier Width in Perovskite Multiple Quantum Wells for High Performance Green Light–Emitting Diodes. Advanced Optical Materials, 2019, 7, 1801575.	7.3	55
53	[M(NMesBMes2)2] (M = Cr, Ni) : Stable, Distorted, Two-Coordinate d4 and d8 Complexes. Angewandte Chemie International Edition in English, 1989, 28, 316-317.	4.4	53
54	Coexistence of Strong Second Harmonic Generation Response and Wide Band Gap in AZn ₄ Ga ₅ S ₁₂ (A=K, Rb, Cs) with 3D Diamondâ€like Frameworks. Chemistry - A European Journal, 2017, 23, 10407-10412.	3.3	53

#	Article	IF	CITATIONS
55	Graphene Dots Embedded Phosphide Nanosheet-Assembled Tubular Arrays for Efficient and Stable Overall Water Splitting. ACS Applied Materials & Interfaces, 2017, 9, 24600-24607.	8.0	52
56	Sr ₅ ZnGa ₆ S ₁₅ : a new quaternary non-centrosymmetric semiconductor with a 3D framework structure displaying excellent nonlinear optical performance. Inorganic Chemistry Frontiers, 2018, 5, 1458-1462.	6.0	51
57	Immobilization of a Molecular Ruthenium Catalyst on Hematite Nanorod Arrays for Water Oxidation with Stable Photocurrent. ChemSusChem, 2015, 8, 3242-3247.	6.8	49
58	Organic Polymer Dots as Photocatalysts for Visible Lightâ€Driven Hydrogen Generation. Angewandte Chemie, 2016, 128, 12494-12498.	2.0	49
59	Design and synthesis of dopant-free organic hole-transport materials for perovskite solar cells. Chemical Communications, 2018, 54, 9571-9574.	4.1	49
60	Recycling spent water treatment adsorbents for efficient electrocatalytic water oxidation reaction. Resources, Conservation and Recycling, 2022, 178, 106037.	10.8	48
61	Regulation of the luminescence mechanism of two-dimensional tin halide perovskites. Nature Communications, 2022, 13, 60.	12.8	48
62	Gas-templating of hierarchically structured Ni–Co–P for efficient electrocatalytic hydrogen evolution. Journal of Materials Chemistry A, 2017, 5, 7564-7570.	10.3	47
63	Construction of Mesoporous Frameworks with Vanadoborate Clusters. Angewandte Chemie - International Edition, 2014, 53, 3608-3611.	13.8	46
64	The Ru-tpc Water Oxidation Catalyst and Beyond: Water Nucleophilic Attack Pathway versus Radical Coupling Pathway. ACS Catalysis, 2017, 7, 2956-2966.	11.2	46
65	Electron Transporting Bilayer of SnO ₂ and TiO ₂ Nanocolloid Enables Highly Efficient Planar Perovskite Solar Cells. Solar Rrl, 2020, 4, 1900331.	5.8	46
66	A comprehensive review on metal chalcogenides with three-dimensional frameworks for infrared nonlinear optical applications. Coordination Chemistry Reviews, 2022, 470, 214706.	18.8	46
67	Pressure-induced semiconductor-to-metal phase transition of a charge-ordered indium halide perovskite. Proceedings of the National Academy of Sciences of the United States of America, 2019, 116, 23404-23409.	7.1	45
68	Oxygen Vacancyâ€Driven Reversible Free Radical Catalysis for Environmentâ€Adaptive Cancer Chemodynamic Therapy. Angewandte Chemie - International Edition, 2021, 60, 20943-20951.	13.8	44
69	Salt-inclusion chalcogenides: an emerging class of IR nonlinear optical materials. Dalton Transactions, 2020, 49, 14338-14343.	3.3	43
70	An electroactive single-atom copper anchored MXene nanohybrid filter for ultrafast water decontamination. Journal of Materials Chemistry A, 2021, 9, 25964-25973.	10.3	43
71	Electrochemical driven water oxidation by molecular catalysts in situ polymerized on the surface of graphite carbon electrode. Chemical Communications, 2015, 51, 7883-7886.	4.1	42
72	Tailored synthesis of nonlinear optical quaternary chalcohalides: Ba ₄ Ge ₃ S ₉ Cl ₂ , Ba ₄ Si ₃ Se ₉ Cl ₂ and Ba ₄ Ge ₃ Se ₉ Cl ₂ . Dalton Transactions, 2017, 46, 2715-2721.	3.3	42

#	Article	IF	CITATIONS
73	Liquid-like Interfaces Mediate Structural Phase Transitions in Lead Halide Perovskites. Matter, 2020, 3, 534-545.	10.0	42
74	Synergistic recycling and conversion of spent Li-ion battery leachate into highly efficient oxygen evolution catalysts. Green Chemistry, 2021, 23, 6538-6547.	9.0	42
75	Converting loess into zeolite for heavy metal polluted soil remediation based on "soil for soil-remediation―strategy. Journal of Hazardous Materials, 2021, 412, 125199.	12.4	42
76	Ba ₅ Cu ₈ In ₂ S ₁₂ : a quaternary semiconductor with a unique 3D copper-rich framework and ultralow thermal conductivity. Chemical Communications, 2017, 53, 2590-2593.	4.1	41
77	Non entrosymmetric Selenides AZn ₄ In ₅ Se ₁₂ (A=Rb, Cs): Synthesis, Characterization and Nonlinear Optical Properties. Chemistry - an Asian Journal, 2017, 12, 453-458.	3.3	41
78	Thermodynamics and crystallization of a theophylline–salicylic acid cocrystal. CrystEngComm, 2015, 17, 4125-4135.	2.6	38
79	Lowâ€Valence Metal Single Atoms on Graphdiyne Promotes Electrochemical Nitrogen Reduction via Mâ€ŧoâ€N ₂ Ï€â€Backdonation. Advanced Functional Materials, 2022, 32, .	14.9	38
80	Catalytic Water Oxidation by a Molecular Ruthenium Complex: Unexpected Generation of a Single-Site Water Oxidation Catalyst. Inorganic Chemistry, 2015, 54, 4611-4620.	4.0	37
81	From Ru-bda to Ru-bds: a step forward to highly efficient molecular water oxidation electrocatalysts under acidic and neutral conditions. Nature Communications, 2021, 12, 373.	12.8	37
82	Improved Performance of Colloidal CdSe Quantum Dot-Sensitized Solar Cells by Hybrid Passivation. ACS Applied Materials & Interfaces, 2014, 6, 18808-18815.	8.0	36
83	Synthesis and structure determination of potassium copper selenide nanowires and solid-state supercapacitor application. Journal of Power Sources, 2014, 268, 522-532.	7.8	36
84	A Cuâ€Based Nanoparticulate Film as Superâ€Active and Robust Catalyst Surpasses Pt for Electrochemical H ₂ Production from Neutral and Weak Acidic Aqueous Solutions. Advanced Energy Materials, 2016, 6, 1502319.	19.5	36
85	Copper(I)-Based Highly Emissive All-Inorganic Rare-Earth Halide Clusters. Matter, 2019, 1, 180-191.	10.0	35
86	Coupled Kinetics of Ferrihydrite Transformation and As(V) Sequestration under the Effect of Humic Acids: A Mechanistic and Quantitative Study. Environmental Science & Technology, 2018, 52, 11632-11641.	10.0	34
87	Defective analcime/geopolymer composite membrane derived from fly ash for ultrafast and highly efficient filtration of organic pollutants. Journal of Hazardous Materials, 2020, 388, 121736.	12.4	34
88	Enhanced Cr(VI) reduction on natural chalcopyrite mineral modulated by degradation intermediates of RhB. Journal of Hazardous Materials, 2022, 423, 127206.	12.4	34
89	Removal of microplastics and nanoplastics from urban waters: Separation and degradation. Water Research, 2022, 221, 118820.	11.3	34
90	PKU-3: An HCl-Inclusive Aluminoborate for Strecker Reaction Solved by Combining RED and PXRD. Journal of the American Chemical Society, 2015, 137, 7047-7050.	13.7	33

#	Article	IF	CITATIONS
91	Mn ₂ O ₃ hollow spheres synthesized based on an ion-exchange strategy from amorphous calcium carbonate for highly efficient trace-level uranyl extraction. Environmental Science: Nano, 2016, 3, 1254-1258.	4.3	32
92	High-efficiency core-shell magnetic heavy-metal absorbents derived from spent-LiFePO4 Battery. Journal of Hazardous Materials, 2021, 402, 123583.	12.4	32
93	Halide Homogenization for High-Performance Blue Perovskite Electroluminescence. Research, 2020, 2020, 9017871.	5.7	32
94	Integrating electrodeposition with electrolysis for closed-loop resource utilization of battery industrial wastewater. Green Chemistry, 2022, 24, 3208-3217.	9.0	32
95	Electronic and Structural Effects of Inner Sphere Coordination of Chloride to a Homoleptic Copper(II) Diimine Complex. Inorganic Chemistry, 2018, 57, 4556-4562.	4.0	31
96	Integrating high-efficiency oxygen evolution catalysts featuring accelerated surface reconstruction from waste printed circuit boards via a boriding recycling strategy. Applied Catalysis B: Environmental, 2021, 298, 120583.	20.2	31
97	Two excellent phase-matchable infrared nonlinear optical materials based on 3D diamond-like frameworks: RbGaSn ₂ Se ₆ and RbInSn ₂ Se ₆ . Dalton Transactions, 2017, 46, 7714-7721.	3.3	30
98	Protonation stabilized high As/F mobility red mud for Pb/As polluted soil remediation. Journal of Hazardous Materials, 2021, 404, 124143.	12.4	30
99	A facile, environmentally friendly synthesis of strong photo-emissive methylammonium lead bromide perovskite nanocrystals enabled by ionic liquids. Green Chemistry, 2020, 22, 3433-3440.	9.0	29
100	Aqueous Organometallic Chemistry. 2. 1H NMR Spectroscopic, Synthetic, and Structural Study of the Chemo- and Diastereoselective Reactions of [Cp*Rh(H2O)3]2+ with Nitrogen Ligands as a Function of pH. Organometallics, 1996, 15, 2009-2013.	2.3	28
101	One-step synthesis of water dispersible silica nanoplates. Chemical Communications, 2013, 49, 1300.	4.1	28
102	Transferring waste red mud into ferric oxide decorated ANA-type zeolite for multiple heavy metals polluted soil remediation. Journal of Hazardous Materials, 2022, 424, 127244.	12.4	28
103	Electrochemical Driven Phase Segregation Enabled Dual-Ion Removal Battery Deionization Electrode. Nano Letters, 2021, 21, 4830-4837.	9.1	27
104	Dipicolinic acid: a strong anchoring group with tunable redox and spectral behavior for stable dye-sensitized solar cells. Chemical Communications, 2015, 51, 3858-3861.	4.1	26
105	A Crystalline Mesoporous Germanate with 48â€Ring Channels for CO ₂ Separation. Angewandte Chemie - International Edition, 2015, 54, 7290-7294.	13.8	26
106	Hollow Iron–Vanadium Composite Spheres: A Highly Efficient Ironâ€Based Water Oxidation Electrocatalyst without the Need for Nickel or Cobalt. Angewandte Chemie, 2017, 129, 3337-3341.	2.0	26
107	Modular design of an efficient heterostructured FeS ₂ /TiO ₂ oxygen evolution electrocatalyst <i>via</i> sulfidation of natural ilmenites. Journal of Materials Chemistry A, 2021, 9, 25032-25041.	10.3	26
108	Water Oxidation Initiated by In Situ Dimerization of the Molecular Ru(pdc) Catalyst. ACS Catalysis, 2018, 8, 4375-4382.	11.2	25

#	Article	IF	CITATIONS
109	Interfacial engineering of CuFeS2 quantum dots viaÂplatinum decoration with enhanced Cr(VI) reduction dynamics under UV-Vis-NIR radiation. Journal of Hazardous Materials, 2022, 421, 126701.	12.4	25
110	Microporous core-shell Co11(HPO3)8(OH)6/Co11(PO3)8O6 nanowires for highly efficient electrocatalytic oxygen evolution reaction. Applied Catalysis B: Environmental, 2019, 259, 118091.	20.2	24
111	Ruthenium Complex-Incorporated Two-Dimensional Metal–Organic Frameworks for Cocatalyst-Free Photocatalytic Proton Reduction from Water. Inorganic Chemistry, 2020, 59, 2379-2386.	4.0	24
112	Towards efficient and robust anodes for water splitting: Immobilization of Ru catalysts on carbon electrode and hematite by in situ polymerization. Catalysis Today, 2017, 290, 73-77.	4.4	22
113	Unlocking the electrocatalytic activity of natural chalcopyrite using mechanochemistry. Journal of Energy Chemistry, 2022, 68, 275-283.	12.9	22
114	Hydroxylamine mediated Fenton-like interfacial reaction dynamics on sea urchin-like catalyst derived from spent LiFePO4 battery. Journal of Hazardous Materials, 2022, 431, 128590.	12.4	22
115	A ruthenium water oxidation catalyst based on a carboxamide ligand. Dalton Transactions, 2016, 45, 3272-3276.	3.3	21
116	Sandwich crystals of butyl paraben. CrystEngComm, 2014, 16, 8863-8873.	2.6	19
117	Syntheses, structures, and thermoelectric properties of ternary tellurides: RECuTe2 (RE = Tb–Er). Inorganic Chemistry Frontiers, 2017, 4, 1273-1280.	6.0	19
118	Bandgap engineering of tetragonal phase CuFeS2 quantum dots via mixed-valence single-atomic Ag decoration for synergistic Cr(VI) reduction and RhB degradation. Chinese Chemical Letters, 2021, 32, 3450-3456.	9.0	19
119	In Situ-Fabricated Perovskite Nanocrystals for Deep-Blue Light-Emitting Diodes. Journal of Physical Chemistry Letters, 2020, 11, 10348-10353.	4.6	18
120	Plastic wastes derived carbon materials for green energy and sustainable environmental applications. , 2022, 1, 34-48.		17
121	Blue-Violet Emission with Near-Unity Photoluminescence Quantum Yield from Cu(I)-Doped Rb ₃ InCl ₆ Single Crystals. Journal of Physical Chemistry Letters, 2021, 12, 7928-7934.	4.6	16
122	Construct Polyoxometalate Frameworks through Covalent Bonds. Inorganic Chemistry, 2015, 54, 8699-8704.	4.0	15
123	Eco-designed electrocatalysts for water splitting: A path toward carbon neutrality. International Journal of Hydrogen Energy, 2023, 48, 6288-6307.	7.1	15
124	Superionic Adjustment Leading to Weakly Temperature-Dependent <i>ZT</i> Values in Bulk Thermoelectrics. Inorganic Chemistry, 2015, 54, 867-871.	4.0	14
125	Solid-State Preparation, Structural Characterization, Physical Properties, and Theoretical Studies of a Series of Novel Rare-Earth Metal Chalcogenides with Unprecedented Closed-Cavities. Crystal Growth and Design, 2019, 19, 444-452.	3.0	14
126	A highly efficient porous conductive polymer electrode for seawater desalination. Journal of Materials Chemistry A, 2020, 8, 11811-11817.	10.3	14

#	Article	IF	CITATIONS
127	Decoding the Complex Free Radical Cascade by Using a DNA Frameworkâ€Based Artificial DNA Encoder. Angewandte Chemie - International Edition, 2021, 60, 10745-10755.	13.8	14
128	Dual-anion etching induced in situ interfacial engineering for high-efficiency oxygen evolution. Chemical Engineering Journal, 2022, 431, 134304.	12.7	14
129	Disorder in Extra-Large Pore Zeolite ITQ-33 Revealed by Single Crystal XRD. Crystal Growth and Design, 2013, 13, 4168-4171.	3.0	13
130	Layered V–B–O polyoxometalate nets linked by diethylenetriamine complexes with dangling amine groups. Dalton Transactions, 2014, 43, 15283-15286.	3.3	13
131	Efficient molecular ruthenium catalysts containing anionic ligands for water oxidation. Dalton Transactions, 2016, 45, 18459-18464.	3.3	12
132	(Cs ₆ Cl) ₆ Cs ₃ [Ga ₅₃ Se ₉₆]: A Unique Long Period-Stacking Structure of Layers Made from Ga ₂ Se ₆ Dimers via Cis or Trans Intralayer Linking. Inorganic Chemistry, 2016, 55, 1014-1016.	4.0	12
133	Cs2InCl5(H2O): A moisture-stable defective double halide perovskite analogue with broadband emission. Materials Letters, 2020, 277, 128280.	2.6	12
134	Converting Spent LiFePO ₄ Battery into Zeolitic Phosphate for Highly Efficient Heavy Metal Adsorption. Inorganic Chemistry, 2021, 60, 9496-9503.	4.0	12
135	The Central Role of Ligand Conjugation for Properties of Coordination Complexes as Hole-Transport Materials in Perovskite Solar Cells. ACS Applied Energy Materials, 2019, 2, 6768-6779.	5.1	11
136	Remediation of Cu-polluted soil with analcime synthesized from engineering abandoned soils through green chemistry approaches. Journal of Hazardous Materials, 2021, 406, 124673.	12.4	11
137	The Structure of a Complex Open-Framework Germanate Obtained by Combining Powder Charge-Flipping and Simulated Annealing. Crystal Growth and Design, 2012, 12, 4853-4860.	3.0	10
138	Alkene Epoxidation Catalysts [Ru(pdc)(tpy)] and [Ru(pdc)(pybox)] Revisited: Revealing a Unique Ru ^{IV} â•O Structure from a Dimethyl Sulfoxide Coordinating Complex. ACS Catalysis, 2015, 5, 3966-3972.	11.2	10
139	Enhanced thermoelectric performance in ternary spinel Cu ₄ Mn ₂ Te ₄ <i>via</i> the synergistic effect of tellurium deficiency and chlorine doping. Dalton Transactions, 2017, 46, 14752-14756.	3.3	10
140	Janus Silica Hollow Spheres Prepared via Interfacial Biosilicification. Langmuir, 2015, 31, 11964-11970.	3.5	9
141	Catalyst–solvent interactions in a dinuclear Ru-based water oxidation catalyst. Dalton Transactions, 2016, 45, 19024-19033.	3.3	9
142	A new type of novel salt-inclusion chalcogenide with ultralow thermal conductivity. Chemical Communications, 2020, 56, 15149-15152.	4.1	9
143	Preparations of N- and P-substituted acetylenes under metal-free conditions. Synthetic Communications, 2016, 46, 1438-1445.	2.1	8
144	Accurate lattice-parameter determination from electron diffraction tomography data using two-dimensional diffraction vectors. Journal of Applied Crystallography, 2018, 51, 982-989.	4.5	8

#	Article	IF	CITATIONS
145	Noninvasive Visualization of Sub-5 mm Orthotopic Hepatic Tumors by a Nanoprobe-Mediated Positive and Reverse Contrast-Balanced Imaging Strategy. ACS Nano, 2022, 16, 897-909.	14.6	8
146	Dual Ions Neutralized and Stabilized Red Mud for Chromium(VI) Polluted Soil Remediation. ACS ES&T Engineering, 2022, 2, 913-923.	7.6	8
147	Controlling Strategies and Technologies of Volatile Organic Compounds Pollution in Interior Air of Cars. , 2010, , .		7
148	CsBi ₄ Te ₆ : a new facile synthetic method and mid-temperature thermoelectric performance. Dalton Transactions, 2016, 45, 11931-11934.	3.3	7
149	Polyaniline-graphite composite film glucose oxidase electrode. Central South University, 2006, 13, 653-657.	0.5	6
150	Numerical simulation for volatile organic compound removal in rotating drum biofilter. Science Bulletin, 2007, 52, 2184-2189.	1.7	6
151	Quaternary Layered Semiconductor Ba ₂ Cr ₄ GeSe ₁₀ : Synthesis, Crystal Structure, and Thermoelectric Properties. Inorganic Chemistry, 2018, 57, 916-920.	4.0	6
152	Approaching the Most Economic Preparation of Hole Transport Layer by Organic Monomolecular Strategy for Efficient Inverted Perovskite Solar Cells. Solar Rrl, 2020, 4, 2000011.	5.8	6
153	Robust topology optimization for structures under thermo-mechanical loadings considering hybrid uncertainties. Structural and Multidisciplinary Optimization, 2022, 65, 1.	3.5	6
154	Engineering AND-Gate Aptamer-Signal Base Conjugates for Targeted Magnetic Resonance Molecular Imaging of Metastatic Cancer. ACS Applied Materials & Interfaces, 2022, 14, 17032-17041.	8.0	6
155	Molecular Dynamics Beyond the Monolayer Adsorption as Derived from Langmuir Curve Fitting. Inorganic Chemistry, 2022, 61, 7804-7812.	4.0	6
156	Salt Concentration-Regulated Desalination Mechanism Evolution in Battery Deionization for Freshwater. ACS Sustainable Chemistry and Engineering, 0, , .	6.7	5
157	Ultralow thermal conductivity in the quaternary semiconducting chalcogenide Cs ₄ [Ho ₂₆ Cd ₇ Se ₄₈] with an unprecedented closed cavity architecture. Inorganic Chemistry Frontiers, 2021, 8, 1049-1055.	6.0	4
158	Electron Transporting Bilayer of SnO ₂ and TiO ₂ Nanocolloid Enables Highly Efficient Planar Perovskite Solar Cells. Solar Rrl, 2020, 4, 2070014.	5.8	3
159	Oxygen Vacancyâ€Driven Reversible Free Radical Catalysis for Environmentâ€Adaptive Cancer Chemodynamic Therapy. Angewandte Chemie, 2021, 133, 21111-21119.	2.0	3
160	Green chemical conversion of large-scale aluminosilicates into zeolites for environmental remediation under carbon-neutral pressure. Current Opinion in Green and Sustainable Chemistry, 2022, 36, 100632.	5.9	3
161	Modulated luminescence of zero-dimensional bimetallic all-inorganic halide clusters. Inorganic Chemistry Frontiers, 2022, 9, 3728-3736.	6.0	3
162	Decoding the Complex Free Radical Cascade by Using a DNA Frameworkâ€Based Artificial DNA Encoder. Angewandte Chemie, 2021, 133, 10840-10850.	2.0	2

#	ARTICLE	IF	CITATIONS
163	Synthesis, structure, and luminescent properties of 2 novel 5-chlorhydroxybenzoate-imidazole metal-organic complexes. Turkish Journal of Chemistry, 2014, 38, 79-87.	1.2	1
164	Rücktitelbild: A Tailor-Made Molecular Ruthenium Catalyst for the Oxidation of Water and Its Deactivation through Poisoning by Carbon Monoxide (Angew. Chem. 15/2013). Angewandte Chemie, 2013, 125, 4370-4370.	2.0	0
165	Carbon Nanotubes: Promoting the Water Oxidation Catalysis by Synergistic Interactions between Ni(OH)2and Carbon Nanotubes (Adv. Energy Mater. 15/2016). Advanced Energy Materials, 2016, 6, .	19.5	0